

Geophysical Research Letters[®]



RESEARCH LETTER

10.1029/2021GL096914

Sensitivity of Melting, Freezing and Marine Ice Beneath Larsen C Ice Shelf to Changes in Ocean Forcing

Lianne C. Harrison^{1,2,3} , Paul R. Holland¹ , Karen J. Heywood² , Keith W. Nicholls¹ , and Alex M. Brisbourne¹ 

¹British Antarctic Survey, Cambridge, UK, ²Centre for Ocean and Atmospheric Sciences, School of Environmental Sciences, University of East Anglia, Norwich, UK, ³Now at Centre for Environment, Fisheries and Aquaculture Science, Lowestoft, UK

Key Points:

- An ocean model with new Larsen C bathymetry shows greatest melting and melt sensitivity where seismic data indicate a deep southern trough
- The calculated marine ice distribution under Larsen C Ice Shelf, based on model melt/freeze rates, is in good agreement with observations
- A reduction in marine ice with ocean warming implies a threat to Larsen C stability, with wide implications for cold-water ice shelves

Supporting Information:

Supporting Information may be found in the online version of this article.

Correspondence to:

L. C. Harrison,
lianne.harrison@cefas.co.uk

Citation:

Harrison, L. C., Holland, P. R., Heywood, K. J., Nicholls, K. W., & Brisbourne, A. M. (2022). Sensitivity of melting, freezing and marine ice beneath Larsen C Ice Shelf to changes in ocean forcing. *Geophysical Research Letters*, 49, e2021GL096914. <https://doi.org/10.1029/2021GL096914>

Received 4 NOV 2021

Accepted 8 FEB 2022

Abstract Observations of surface lowering on Larsen C Ice Shelf (LCIS), Antarctica, have prompted concern about its stability. In this study, an ocean model is used to investigate the extent to which changes in ocean forcing may have influenced ice loss and the distribution of stabilizing marine ice beneath LCIS. The model uses a new bathymetry, containing a southern seabed trough discovered using seismic observations. The modeled extent of marine ice, thought to stabilize LCIS, is in good agreement with observations. Experiments applying idealized ocean warming yield an increase in melting over the southern trough. This is inconsistent with lowering observed in northern LCIS, suggesting oceanic forcing is not responsible for that signal. The marine ice extent and thickness reduces significantly under ocean warming, implying a high sensitivity of LCIS stability to changes in ocean forcing. This result could have wide implications for other cold-water ice shelves around Antarctica.

Plain Language Summary Satellite observations have revealed a lowering in recent decades of the surface of Larsen C Ice Shelf (LCIS), Antarctica, which has led to concern about its stability. By modeling ocean conditions under LCIS, we investigate the extent to which ocean melting may have caused the ice to thin, leading to the observed lowering, or altered the pattern of marine ice beneath LCIS. Marine ice forms when seawater freezes to the base of the ice shelf, and is thought to stabilize LCIS. The model uses a new seabed data set that contains a wide, deep seabed trough in the south, found by a seismic survey. In modeled ocean warming experiments, an increase in melting is concentrated in this southern region. However, greater lowering has been observed in the north, suggesting that changes in ocean conditions are not responsible for the lowering. The calculated pattern of marine ice at the base of LCIS looks similar to the observed pattern. With a warmer ocean, marine ice is significantly reduced in crucial regions of the ice shelf. This shows that the stability of LCIS is sensitive to changes in ocean conditions and other ice shelves around Antarctica are likely sensitive to these changes too.

1. Introduction

Amongst long-term temperature variability over the Antarctic Peninsula (Mulvaney et al., 2012), there is ample evidence that this region warmed rapidly in the second half of the 20th century (Vaughan et al., 2003), coinciding with the loss of several ice shelves (Skvarca et al., 1998). Despite a recent warming hiatus (Turner et al., 2016), many have speculated that this trend of ice shelf collapse may result in the loss of the largest ice shelf on the peninsula, Larsen C Ice Shelf (LCIS). The collapse of LCIS would allow an acceleration of grounded glaciers, resulting in an estimated 4.2 mm sea-level rise by 2300 (Schannwell et al., 2018) and a freshening of Antarctic Bottom Water in the Weddell Sea (Jullion et al., 2013).

Oceanic basal melting is one possible cause of the surface lowering of LCIS observed by satellite altimetry (Shepherd et al., 2003). Holland et al. (2015) determined that both ice loss (which they defined as from ice divergence and/or basal melting) and air loss (from the surface firn layer) had contributed to the surface lowering, meaning at least two types of forcing are responsible. Estimates of LCIS basal melt rates from modeling and observations range from 0.1 to 1.3 m/yr (Adusumilli et al., 2018; Borstad et al., 2013; Davis & Nicholls, 2019a; Holland et al., 2009, 2015; Mueller et al., 2012; McGrath et al., 2014). These values include shelf-wide averages and measurements from a single location, over a range of different time periods. There is little consensus on the spatial pattern of basal melting, with some studies showing melting concentrated mainly along the grounding line

© 2022. The Authors.

This is an open access article under the terms of the [Creative Commons Attribution License](https://creativecommons.org/licenses/by/4.0/), which permits use, distribution and reproduction in any medium, provided the original work is properly cited.

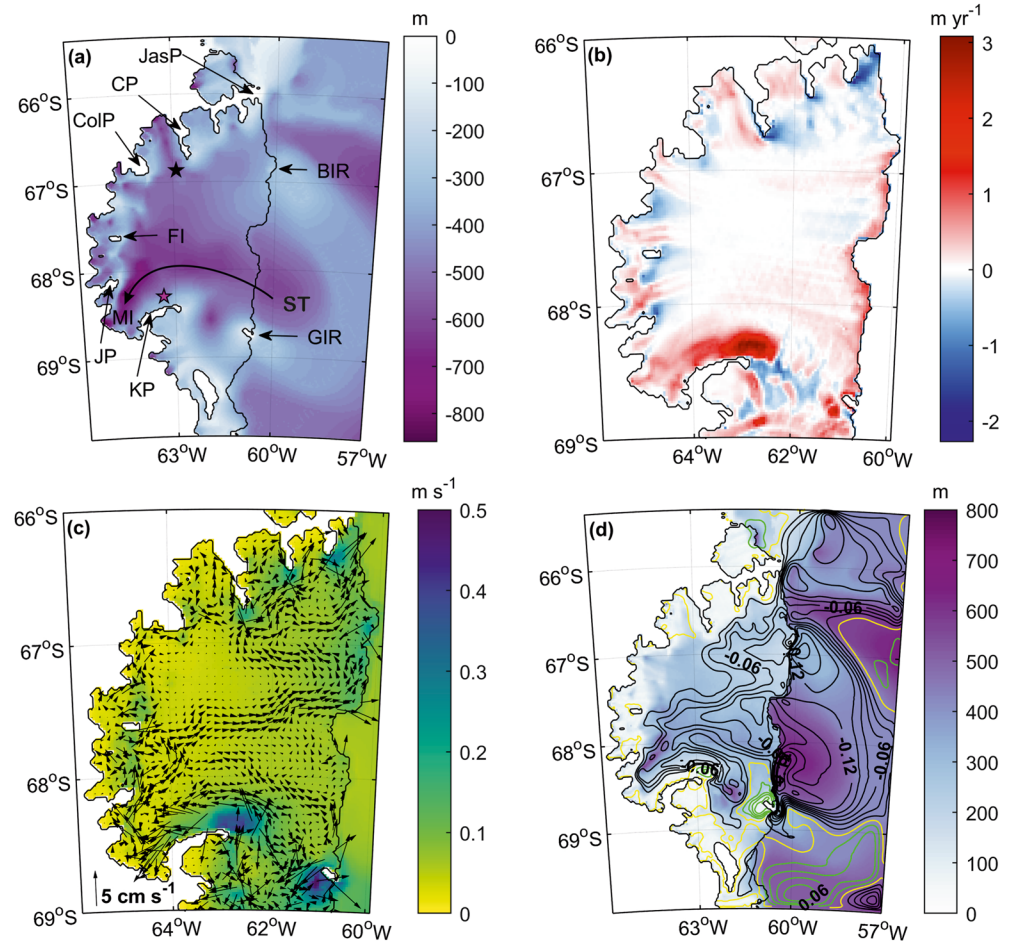


Figure 1. (a) New bathymetry used in model simulations: JasP-Jason Peninsula; CP-Churchill Peninsula; ColP-Cole Peninsula; JP-Joerg Peninsula; KP-Kenyon Peninsula; BIR-Bawden Ice Rise; GIR-Gipps Ice Rise; FI-Francis Island; MI-Mobiloil Inlet; ST-southern trough. Stars indicate mooring sites. (b) Melt rate pattern in the “standard run”; red shows melting, blue shows refreezing. (c) Current speeds (color) and annual-mean velocities (vectors) at the ice shelf base. Every third vector is plotted and vectors larger than 5 cm/s are removed for clarity. (d) Water-column thickness with barotropic streamfunction contours from the standard run overlaid. Contour spacing is 0.02 Sv with negative values (clockwise flow) shown in black, positive (anticlockwise) in green, and the zero contour in yellow.

(Adusumilli et al., 2020; Borstad et al., 2013; Holland et al., 2009), and others showing greatest melting around Bawden Ice Rise (Figure 1a) in the northeast (McGrath et al., 2014; Mueller et al., 2012).

Whether or not basal melting is contributing to the observed surface elevation changes, LCIS is vulnerable to ocean changes through its marine ice. Buoyant meltwater rising under an ice shelf may become supercooled as a result of the pressure-induced increase in the freezing point, causing marine ice to form on the ice base (Holland et al., 2009; Robin, 1979). Under this supercooling, tiny frazil ice crystals form a slushy layer that compacts upwards under buoyancy forces (Oerter et al., 1992). Thick bands of marine ice are found under many cold-water ice shelves, including Filchner-Ronne (Lambrecht et al., 2007), Ross (Neal, 1979) and Amery ice shelves (Fricker et al., 2001), and are thought to impose an important stabilizing effect by binding ice flow units together (Craven et al., 2009; Grosfeld et al., 1998; Oerter et al., 1992).

Marine ice is also thought to stabilize LCIS (Holland et al., 2009; Jansen et al., 2013; Kulesa et al., 2019), as evidenced by the deceleration and termination of rifts in suture zones between ice flow units (Glasser et al., 2009; Holland et al., 2009; Jansen et al., 2015). Borstad et al. (2017) speculated that the stability of LCIS depends on the Joerg Peninsula (Figure 1a) marine ice band, which arrested dozens of rifts until a rift recently penetrated the band and calved iceberg A68 (Hogg & Gudmundsson, 2017; Jansen et al., 2015). The basally-accumulated marine ice investigated here is not the only type of marine ice which may be present on LCIS. Two additional

types of marine ice form as frozen seawater in the surface firn layer, accumulated when this layer dips below sea level, and sea ice within ice shelf rifts, which acts in a similar way to fast ice at calving fronts, compacting and healing fractures (Holland et al., 2009). Here we only consider basally-accreted marine ice. Weakening of LCIS marine ice, by either an increase in basal melting of marine ice bands or simply a reduction in oceanic freezing, may decouple ice flow units with different ice velocities (Jansen et al., 2010), leaving unstable stress fields (Kulesa et al., 2014). Any reduction in marine ice extent or thickness may also enhance the propagation of rifts (Borstad et al., 2017; Larour et al., 2021). The timescales across which marine ice can affect the stability of LCIS are uncertain as a result of the different processes at play.

The continental shelf offshore of LCIS is predominantly covered by sea ice, so there are few ship-based observations of ocean conditions (Bathmann et al., 1994; Huhn et al., 2008; Nicholls et al., 2004). Sparse direct observations within the ice shelf cavity, obtained through boreholes, show that currents are dominated by tides (Davis & Nicholls, 2019a; Nicholls et al., 2012), and ocean models have further highlighted the important role tides play in controlling ocean circulation and melting (Mueller et al., 2012). Nicholls et al. (2004, 2012) suggested that High Salinity Shelf Water, generated by sea ice formation over the continental shelf, enters the LCIS cavity around Gipps Ice Rise. After interaction with the ice near Kenyon Peninsula, this inflow reaches the grounding line at Mobiloil Inlet. Outflow from the cavity has been observed in the north of LCIS, at Jason Peninsula (Nicholls et al., 2004). Model simulations suggest this outflow represents a central plume that gathers meltwater from all along the grounding line (Holland et al., 2009). Two borehole sites (stars in Figure 1a) showed the entire water column to be below the surface freezing point, with little variability in temperature and salinity with depth (Nicholls et al., 2012). Year-long timeseries of ocean temperature, salinity and melting at the southern borehole site show no clear seasonal cycle (Davis & Nicholls, 2019b).

The sparse observational record means it is not possible to determine whether past changes in ocean melting could account for ice shelf thinning or any reduction in marine ice. In this study, we investigate the response of ice shelf melting, freezing and marine ice to changes in ocean forcing using a high-resolution ocean model with a newly-observed bathymetry data set.

2. Methods

We ran simulations using the MITgcm ocean model, including an ice shelf with steady thickness (Losch, 2008; Marshall et al., 1997). The domain includes the LCIS cavity and a small area of the western Weddell Sea (Figure 1a), with a uniform grid resolution of 20 m in the vertical, $1/20^\circ$ in longitude, and variable in latitude, scaled by the cosine of the latitude, resulting in isotropic grid cells of ~ 2 km width. We use constant diffusivities of $10 \text{ m}^2/\text{s}$ in the horizontal and $10^{-4} \text{ m}^2/\text{s}$ in the vertical, and lateral and vertical eddy viscosity coefficients of $50 \text{ m}^2/\text{s}$ and $10^{-3} \text{ m}^2/\text{s}$, respectively, following Holland (2017). Higher values were chosen for viscosity coefficients than diffusivity values for the sake of numerical stability.

A three-equation model is used to parameterize melting and freezing, with a drag coefficient ($c_d = 0.0022$) derived from LCIS observations (Davis & Nicholls, 2019a) and heat and salt transfer coefficients ($\gamma_T = 0.011$, $\gamma_S = 3.1 \times 10^{-4}$) from Jenkins et al. (2010). Frazil ice is not included in the model to save computational expense. Marine ice growth is represented solely by the three-equation parameterization, freezing directly to the ice base when the ocean becomes supercooled. Direct freezing has been found to compensate for a neglect of frazil in models (Jenkins & Bombosch, 1995). Using this approach, we expect the general location of freezing to be accurate, while the exact freezing rates are less certain (Holland & Feltham, 2006; Jenkins & Bombosch, 1995).

Ice topography is sourced from Bedmap2 (Fretwell et al., 2013). A new bathymetry data set (hereafter referred to as the “Brisbourne” bathymetry, Figure 1a) was created, using natural neighbor interpolation of 114 seismic soundings of the LCIS cavity (Brisbourne et al., 2020). To ensure that the combination of these two data sets did not artificially ground ice, we deepened the bathymetry to create a minimum water-column thickness of 40 m, the thickness of two full grid cells, to allow unhindered flow wherever the ice is known to be floating.

Tides are implemented by imposing velocities on open boundaries to the north, east and south from the CATS2008 inverse tidal model (Howard et al., 2019). No other velocity boundary conditions are applied, so currents in the model are driven solely by tides and thermohaline processes. The model domain is too small to represent all the complex processes occurring in the Weddell Sea, so we neglect all surface forcing and instead force the model in

an idealized fashion by prescribing constant ocean properties on the model boundaries. Sea ice formation over the continental shelf constrains water masses here to the surface freezing point, so the “standard run” uses a potential temperature of -1.9°C and practical salinity of 34.5 for its initial and boundary conditions.

Further simulations with initial and boundary condition temperatures of -1.8°C , -1.6°C , and -1.4°C were run to test the sensitivity of LCIS to changes in ocean forcing. The upper bound was chosen to match summertime observations in front of the ice shelf (Bathmann et al., 1994; Nicholls et al., 2004). Unless otherwise stated, all results are averaged over the final year of a 10-year simulation, when the model had reached steady state.

3. Results and Discussion

3.1. Standard Run: Melting, Freezing and Cavity Circulation

The model produced the greatest long-term mean melt rate (~ 3 m/yr) just north of the tip of Kenyon Peninsula (Figure 1b). There is a single direct observation with which to validate the modeled melting; a mooring in the south of LCIS (Nicholls et al. (2012); pink star in Figure 1a) recorded mean melting of 0.7 m/yr with a standard deviation of 1 m/yr (Davis & Nicholls, 2019a). At 1.2 m/yr, modeled melting at this location is within the range of variability. Mean modeled speeds at the mooring location of 0.13 m/s are higher than the observation of 0.09 m/s (Davis & Nicholls, 2019b), explaining the higher modeled melt rate, which is dependent on flow speeds adjacent to the ice. Regions of strong melting and freezing coincide with the highest near-ice current speeds of up to 0.5 m/s (Figures 1b and 1c) in areas of shallow water-column thickness (Figure 1d), where tidal mixing of heat toward and away from the ice base supports both melting and freezing processes, respectively. All speeds reported in this study are the time-average over 180 days of hourly speeds (therefore including the effect of tides) from an extension of the standard run.

The greatest freezing takes place south of Jason Peninsula (Figure 1b), in a location of shallow water-column thickness and high near-ice current speeds (Figures 1c and 1d), where a plume of cold, fresh meltwater exits the cavity (Figure 1c). Freezing also occurs offshore of all peninsulas and islands, which compares well with freezing locations found by Holland et al. (2009) (see Supporting Information S1 for further information).

Ocean currents enter the cavity at Gipps Ice Rise, as suggested by Nicholls et al. (2004, 2012), and exit south of Jason Peninsula (Figure 1d), in agreement with Nicholls et al. (2004), Holland et al. (2009) and Mueller et al. (2012). The new seabed data set contains observations of a trough in the deep southern LCIS cavity (Figure 1a). This “southern trough” deflects inflowing currents, at $\sim 68^{\circ}\text{S}$, as well as steering a northward meltwater flow. Near-ice velocities indicate a meltwater plume that originates from enhanced melting in Mobiloil Inlet and travels northward to Francis Island (Figure 1c). Here, a shallower seabed thins the water column, redirecting the plume eastward, as suggested by Brisbourne et al. (2014), along the northern flank of the southern trough at $\sim 67.5^{\circ}\text{S}$.

Modeled tides are in good agreement with available observations (see Supporting Information S1). Tidal rectification was shown by Mueller et al. (2012) to be an important driving mechanism for cavity circulation, which is confirmed by our model. However, while Mueller et al. (2012) found rectified tides were stronger than thermohaline-driven currents in the northeast of the cavity, the main residual flow in our model occurs in the southern trough (see Figure S2 in the Supporting Information S1). Rectified currents are an important component of the time-mean circulation, advecting water masses along the southern trough and supporting high melt rates in this region. In addition, turbulent mixing of heat toward/away from the ice base, dictated by instantaneous tidal current speeds, has an important control over melting and freezing.

3.2. Effect of Bathymetry

Our LCIS simulations are the first to use a seabed constrained by in-cavity observations. To explain the influence of the improved bathymetry (Figure 2a), two further simulations were performed. A simulation using Bedmap2 bathymetry (Figure 2b) produced similar melting/freezing to the standard run, but with an altered ocean circulation (Figures 2d and 2e). The plume originating in Mobiloil Inlet travels more directly north (i.e., remaining further west) than in the standard run because of the relatively flat Bedmap2 seabed; its path more closely resembles that of Holland et al. (2009) who used a two-dimensional plume model with no influence of bathymetry. Mueller et al. (2012) found a significantly different LCIS melt pattern, including rapid melting around Bawden

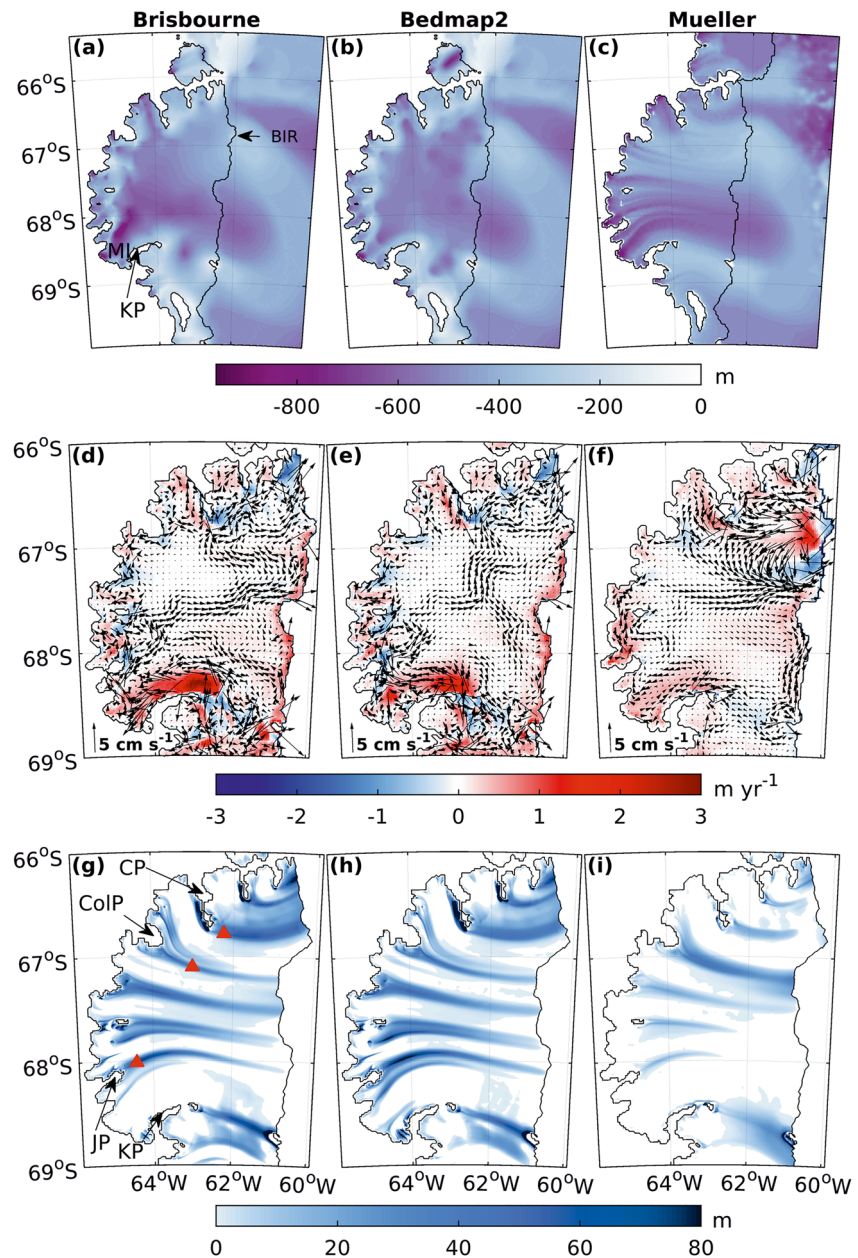


Figure 2. Bathymetries used in simulations: from (a) Brisbane et al. (2020), (b) Fretwell et al. (2013) (Bedmap2), and (c) Mueller et al. (2012). (d–f) Corresponding melt rates and annual-mean velocities directly beneath ice shelf base. (g–i) Illustrative marine ice thickness for each bathymetry case after advecting ocean model melt and freeze rates using constant ice velocities for a period of 500 years, approximately the residence time of ice in LCIS. Red triangles show locations of marine ice thickness comparisons with observations, as detailed in text.

Ice Rise. Applying the Mueller geometry (bathymetry and ice topography created by Mueller et al. (2012), Figure 2c) to our model dramatically increases melting around Bawden Ice Rise, with the thinner water column in the northern cavity resulting in much higher mean velocities (Figure 2f) and tidal speeds (Figure S3 in the Supporting Information S1).

These simulations demonstrate how imperative the bathymetry is for modeled LCIS ocean circulation and melt/freeze rates. The Bedmap2 and Mueller bathymetries are not constrained by observations in the cavity, so the circulation and melt/freeze patterns in our standard run are expected to be most realistic. One way to test this is to examine the marine ice distributions that are implicit in the melt/freeze patterns.

3.3. Marine Ice

To consider the influence of ocean melt/freeze patterns on ice-shelf stability, we investigated hypothetical steady-state marine ice thickness fields produced using the melting and freezing results of each simulation (Figures 2g–2i). This calculation assumes that modeled melt/freeze rates, and ice shelf velocities (Mouginot et al., 2012; Rignot et al., 2011), are fixed in time. These fields are interpolated onto a 100-m grid and then marine ice thickness is time-stepped on this grid for 500 years (approximately the residence time of ice in LCIS (Glasser et al., 2009)) using a simple upwind advection scheme. High spatial resolution is used to minimize numerical diffusion. These marine ice fields are purely illustrative, since the 500-year steady-state assumption is unlikely to hold. Model melting and freezing are also highly uncertain, as a result of limitations in modeled ocean circulation, temperature and melting, and the lack of a frazil ice model. Nevertheless, the standard run produces a marine ice distribution (Figure 2g) that is very similar to observations (Holland et al. (2009); see Figure S5 in Supporting Information S1).

The thickness of marine bands calculated in this study is up to ~80 m, with bands being thinned toward the calving front by melting and ice divergence, in accordance with observations (Brisbourne et al., 2014). Jansen et al. (2013) found the mean thickness of the Joerg Peninsula marine band close to the grounding line to be 100–200 m, whereas we calculated a marine ice thickness of ~80 m in a comparable location (see southernmost red triangle in Figure 2g), which suggests that freezing rates simulated here may be too low, possibly due to the lack of frazil ice in the model. McGrath et al. (2014) reported thicknesses of Churchill Peninsula and Cole Peninsula marine bands of 56 ± 25 m and 26 ± 9 m, respectively. Thicknesses produced by our model at those locations (remaining red triangles in Figure 2g) were ~50 m near Churchill Peninsula and ~40 m in the Cole Peninsula marine ice band. All of these values show reasonable agreement with observations, considering the uncertainty in modeled freezing rates and the calculation of marine ice bands.

The marine ice distribution produced using the Bedmap2 run (Figure 2h) shows a very similar pattern to the standard run (Figure 2g), particularly in the northern half of LCIS. In the south, the marine ice bands are slightly thinner in the standard run, as a result of its higher melt rates. Marine ice distribution in the Mueller case (Figure 2i) is greatly reduced in both thickness and extent compared with the Brisbourne pattern. Marine ice bands in the south of the Mueller domain only reach approximately halfway across the ice shelf, and the Churchill Peninsula band in the north, which has been identified as important to LCIS stability (McGrath et al., 2014), also does not extend to the ice front. This field qualitatively disagrees with the observations of Holland et al. (2009), which are shown in Figure S5b in the Supporting Information S1.

This analysis illustrates the importance of the new bathymetry data set, and shows that the standard run is suitable to test the sensitivity of predicted marine ice distributions.

3.4. Sensitivity to Ocean Warming

We wanted to explore the influence of ocean warming on the marine ice distribution beneath LCIS, and whether ocean changes may be responsible for the observed surface lowering. To this end, we first investigated the difference in steady melt/freeze rates between the standard run and a series of warmer runs, before examining the predicted steady-state marine ice distributions for these simulations.

3.4.1. Melt Rate Changes

The largest increase in absolute melt rate when ocean temperatures are raised coincides with the regions of greatest melting, in southern LCIS, at Kenyon Peninsula and Gipps Ice Rise (Figures 3a–3d). However, the greatest observed surface lowering has occurred in the north, where atmospheric warming was reported to be greatest during the 20th century (Vaughan et al., 2003). The discrepancy between these two lines of evidence suggests that the lowering is influenced more by surface processes than basal processes. Note, however, that these results reflect the response to a spatially and temporally-uniform ocean warming. If greater ocean warming occurred in the north of LCIS, or complex seasonal or inter-annual temperature variability occurred, the melting response may differ. Holland et al. (2015) combined ice elevation and radar data to determine that ice loss, rather than firn densification, was the dominant contributor to lowering over the southernmost portion of their survey line, which covered Mobiloil Inlet. Our results suggest that this signal might reflect a local ocean-driven melting increase.

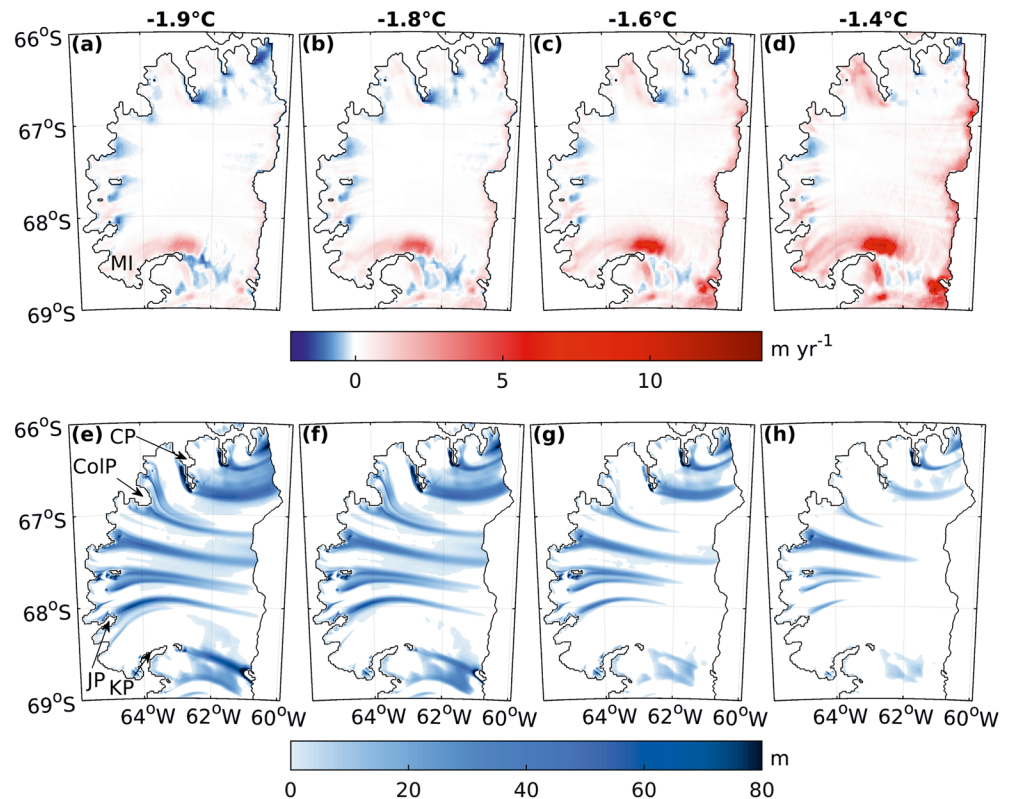


Figure 3. (a–d) Melt/freezing pattern and (e–h) illustrative marine ice thickness for different ocean temperature cases.

Mueller et al. (2012) reported a 0.2 m/yr increase in shelf-wide melt rate with a change in ocean temperature from -1.9°C to -1.7°C , a sensitivity replicated here. When ocean temperatures were raised from -1.9°C to -1.4°C in the study of Holland et al. (2009), the average melt rate increased by 1 m/yr, whereas here melting only increased by 0.8 m/yr with the same ocean warming. Their deep ocean was warmed directly beneath the plume layer, whereas our three-dimensional model is subjected to warm waters at the lateral boundaries, with the waters cooling as they progress through the domain to reach the ice. This suggests that LCIS may be protected from ocean warming by negative feedbacks within the cavity, for example, through tidal mixing with cooler meltwater.

3.4.2. Marine Ice Changes

Even after a temperature increase of 0.5°C , basal freezing still occurs offshore of all islands and peninsulas (Figure 3d). However, freezing rates are significantly reduced, notably at Joerg and Cole peninsulas, which generate marine ice bands that are particularly important for curtailing rift propagation in LCIS (McGrath et al., 2014). As ocean temperatures increase, inferred marine ice distributions are progressively thinned and reduced in extent (Figures 3e–3h). With an ocean temperature increase to -1.4°C , reduced freezing at Joerg Peninsula and enhanced melting downstream leads to a significant reduction in the extent of its marine ice band. With this marine ice band no longer extending beyond the tip of Kenyon Peninsula, the rifts emanating from this region may be able to propagate into the center of LCIS and trigger significant ice shelf retreat. Furthermore, in this warmest simulation no marine ice bands reach the present-day calving front, suggesting widespread destabilization.

While we do not analyze the influence of marine ice on ice shelf stability, there is good evidence that these marine ice bands inhibit fracture propagation and prevent this rifted ice shelf from disintegrating (Borstad et al., 2017; Holland et al., 2009; Jansen et al., 2013, 2015; Kulesa et al., 2019). Marine ice also limits the propagation of rifts in the Amery Ice Shelf (Bassis et al., 2007; Heeszel et al., 2014), suggesting its ice front would retreat if this marine ice were diminished under changing ocean conditions. Thus, the results of this study may be widely applicable to other cold-water Antarctic ice shelves. Ice shelf retreat at calving fronts is particularly influential where the ice flow is supported by pinning points such as Bawden Ice Rise (Borstad et al., 2013). The removal of such

ice can result in unstable geometries and lead to complete ice shelf collapse, as was predicted prior to the collapse of Larsen B Ice Shelf in 2002 (Doake et al., 1998).

If ocean warming were to occur in the LCIS cavity, any resulting reduction in accumulation of marine ice at the grounding line, which might weaken the ice shelf, would take several centuries to advect to areas closer to the ice front that are threatened by rifting. By contrast, a change in melting could directly thin existing marine ice bands much more rapidly. Freezing across LCIS appears to be relatively insensitive to ocean forcing changes, whereas melting increased significantly with the same changes (Figures 3a–3d). We therefore expect the dominant process of marine ice retreat to be increased melting rather than decreased freezing. However, this analysis is subject to the lack of frazil ice in our ocean model. These results demonstrate substantial uncertainty in the timescales needed for ocean temperature changes to affect LCIS stability, and highlight that the present-day marine ice configuration is the result of centuries of ocean melt/freeze and ice flow conditions.

Note that the marine ice observed in LCIS may include contributions from rift mélange or seawater-flooded firn, in addition to the basally-accreted ice represented by our model (McGrath et al., 2014; Kulesa et al., 2019). The formation of these other types of marine ice would be expected to have a different sensitivity to any climate changes. However, the widespread increases in basal melting found in our experiments imply that marine ice bands would be thinned and retreated by ocean warming, regardless of their formation mechanism.

4. Conclusions

We have presented results from a high-resolution model of ocean processes in the LCIS cavity, using a new bathymetry created using seismic soundings. The highest mean melt rates were found just north of Kenyon Peninsula, where the improved representation of a southern trough directs inflowing currents to the grounding line. This result contrasts with earlier simulations that used different bathymetric data sets. Melt/freeze results from this new model have been used to construct a steady-state prediction of the marine ice pattern at the base of LCIS, which is in agreement with observations. We conducted ocean warming experiments to assess how the cavity could respond to changes in ocean forcing on the continental shelf. With uniform warming, greater increases in basal melting occur in the vicinity of the southern trough, suggesting that satellite-observed lowering in the north of LCIS is more likely the result of surface processes than basal melting changes.

These warming experiments also reveal changes in ocean freezing at the base of LCIS, and we examined the impact of these changes on predicted steady-state marine ice thicknesses. A strong reduction in the Joerg Peninsula marine ice band is found when the ocean is warmed, which could destabilize LCIS if higher temperatures endure. The imposed ocean warming also causes other marine ice bands to terminate before reaching the ice front, further suggesting a general retreat of LCIS might occur. This result has implications for other cold-water Antarctic ice shelves, such as Filchner-Ronne or Amery ice shelves, that may be susceptible to destabilization by a reduction in the thickness or extent of marine ice bands in response to ocean warming (Craven et al., 2009; Grosfeld et al., 1998; Oerter et al., 1992).

Future work is needed to sample the marine ice in LCIS and determine what fraction is comprised of the basally-accreted ice examined here. Further advances in the oceanography of the LCIS cavity require additional measurements to better constrain the seabed, and additional sub-ice observations to quantify ocean processes and validate models. Coupling of ocean and ice sheet models (including a marine ice component) would also be invaluable to our understanding of the sensitivity of LCIS to changes in ocean forcing.

One important implication of our results is that the timescales needed for ocean change to affect LCIS stability are asymmetric: a change in freezing would take centuries to propagate through the ice shelf, while a change in melting could thin existing marine ice bands rapidly. This means that the overall timescale of the response to an ocean change is highly uncertain.

Data Availability Statement

The model output underlying the figures and calculations in this paper is available through the UK Polar Data Centre (<https://doi.org/10.5285/A54C795C-E0EE-49CB-99DD-BEFBDC4A70F0>).

Acknowledgments

This work was supported by the Natural Environment Research Council and the EnvEast Doctoral Training Partnership [Grant No. NE/L002582/1] and PICCOLO [Grant No. NE/P021395/1]. The authors would like to thank all contributors to the LCIS seabed data set, and would also like to thank R. Mueller for sharing her LCIS model geometry. Additionally, we thank L. Padman, J. Graham and one anonymous reviewer for their help improving the manuscript.

References

Adusumilli, S., Fricker, H. A., Medley, B., Padman, L., & Siegfried, M. R. (2020). Interannual variations in meltwater input to the Southern Ocean from Antarctic ice shelves. *Nature Geoscience*, 13(9), 616–620. <https://doi.org/10.1038/s41561-020-0616-z>

Adusumilli, S., Fricker, H. A., Siegfried, M. R., Padman, L., Paolo, F. S., & Ligtenberg, S. R. M. (2018). Variable basal melt rates of Antarctic peninsula ice shelves, 1994–2016. *Geophysical Research Letters*, 45(9), 4086–4095. <https://doi.org/10.1002/2017gl076652>

Bassis, J. N., Fricker, H. A., Coleman, R., Bock, Y., Behrens, J., Darnell, D., et al. (2007). Seismicity and deformation associated with ice-shelf rift propagation. *Journal of Glaciology*, 53(183), 523–536. <https://doi.org/10.3189/002214307784409207>

Bathmann, U., Smetacek, V., de Baar, H., Fahrbach, E., & Krause, G. (1994). *The expeditions ANTARKTIS X/6-8 of the research vessel "POLARSTERN" in 1992/93, report*. Alfred-Wegener Inst.

Borstad, C., McGrath, D., & Pope, A. (2017). Fracture propagation and stability of ice shelves governed by ice shelf heterogeneity. *Geophysical Research Letters*, 44(9), 4186–4194. <https://doi.org/10.1002/2017gl072648>

Borstad, C., Rignot, E., Mougnot, J., & Schodlok, M. P. (2013). Creep deformation and buttressing capacity of damaged ice shelves: Theory and application to larsen C ice shelf. *The Cryosphere*, 7, 1931–1947. <https://doi.org/10.5194/tc-7-1931-2013>

Brisbourne, A., Kullessa, B., Hudson, T., Harrison, L., Holland, P., Luckman, A., & Smith, A. (2020). An updated seabed bathymetry beneath larsen C ice shelf, Antarctic peninsula. *Earth System Science Data*, 12(2), 887–896. <https://doi.org/10.5194/essd-12-887-2020>

Brisbourne, A., Smith, A., King, E., Nicholls, K., Holland, P., & Makinson, K. (2014). Seabed topography beneath larsen C ice shelf from seismic soundings. *The Cryosphere*, 8, 1–13. <https://doi.org/10.5194/tc-8-1-2014>

Craven, M., Allison, I., Fricker, H. A., & Warner, R. (2009). Properties of a marine ice layer under the Amery ice shelf, East Antarctica. *Journal of Glaciology*, 55(192), 717–728. <https://doi.org/10.3189/002214309789470941>

Davis, P. E. D., & Nicholls, K. W. (2019a). Turbulence observations beneath larsen C ice shelf, Antarctica. *Journal of Geophysical Research: Oceans*, 124(8), 5529–5550. <https://doi.org/10.1029/2019jc015164>

Davis, P. E. D., & Nicholls, K. W. (2019b). *Turbulence observations beneath larsen C ice shelf, Antarctica*. Polar Data Centre, Natural Environment Research Council. <https://doi.org/10.5285/16ee2665-d0d0-41b9-a046-23b0a7369c61>

Doake, C., Corr, H., Rott, H., Skvarca, P., & Young, N. (1998). Breakup and conditions for stability of the northern larsen ice shelf, Antarctica. *Nature*, 391(6669), 778–780. <https://doi.org/10.1038/35832>

Fretwell, P., Pritchard, H. D., Vaughan, D. G., Bamber, J. L., Barrand, N. E., & Bell, R. (2013). Bedmap2: Improved ice bed, surface and thickness datasets for Antarctica. *The Cryosphere*, 7, 375–393. <https://doi.org/10.5194/tc-7-375-2013>

Fricker, H. A., Popov, S., Allison, I., & Young, N. (2001). Distribution of marine ice beneath the Amery ice shelf. *Geophysical Research Letters*, 28(11), 2241–2244. <https://doi.org/10.1029/2000gl012461>

Glasser, N. F., Kullessa, B., Luckman, A., Jansen, D., King, E. C., Sammonds, P. R., & Jezek, K. C. (2009). Surface structure and stability of the Larsen C ice shelf, Antarctic Peninsula. *Journal of Glaciology*, 55(191), 400–410. <https://doi.org/10.3189/002214309788816597>

Grosfeld, K., Hellmer, H., Jonas, M., Sandhäger, H., Schulte, M., & Vaughan, D. G. (1998). Marine ice beneath Filchner Ice Shelf: Evidence from a multi-disciplinary approach. Ocean, ice and atmosphere Interactions at the Antarctic continental margin. In S. Jacobs, & R. Weiss (Eds.), *Antarct res ser* (Vol. 75, pp. 319–339). AGU. <https://doi.org/10.1029/AR075p0319>

Heeszel, D. S., Fricker, H. A., Bassis, J. N., O’Neel, S., & Walter, F. (2014). Seismicity within a propagating ice shelf rift: The relationship between icequake locations and ice shelf structure. *Journal of Geophysical Research: Earth Surface*, 119(4), 731–744. <https://doi.org/10.1002/2013jf002849>

Hogg, A. E., & Gudmundsson, G. H. (2017). Impacts of the larsen-C ice shelf calving event. *Nature Climate Change*, 7(8), 540–542. <https://doi.org/10.1038/nclimate3359>

Holland, P. R. (2017). The transient response of ice shelf melting to ocean change. *Journal of Physical Oceanography*, 47(8), 2101–2114. <https://doi.org/10.1175/jpo-d-17-0071.1>

Holland, P. R., Brisbourne, A., Corr, H. F. J., McGrath, D., Purdon, K., Paden, J., & Fleming, A. H. (2015). Oceanic and atmospheric forcing of Larsen C Ice Shelf thinning. *The Cryosphere*, 9, 1005–1024. <https://doi.org/10.5194/tc-9-1005-2015>

Holland, P. R., Corr, H. F. J., Vaughan, D. G., & Jenkins, A. (2009). Marine ice in larsen ice shelf. *Geophysical Research Letters*, 36(11). <https://doi.org/10.1029/2009gl038162>

Holland, P. R., & Feltham, D. L. (2006). The effects of rotation and ice shelf topography on frazil-laden ice shelf water plumes. *Journal of Physical Oceanography*, 36(12), 2312–2327. <https://doi.org/10.1175/jpo2970.1>

Howard, S. L., Padman, L., & Erofeeva, S. (2019). *CATS2008: Circum-Antarctic tidal simulation version 2008 U.S. Antarctic program (USAP) data center*. <https://doi.org/10.15784/601235>

Huhn, O., Hellmer, H. H., Rhein, M., Rodehacke, C., Roether, W., Schodlok, M. P., & Schröder, M. (2008). Evidence of deep-and bottom-water formation in the western Weddell Sea. *Deep Sea Research Part II: Topical Studies in Oceanography*, 55(8–9), 1098–1116. <https://doi.org/10.1016/j.dsr2.2007.12.015>

Jansen, D., Kullessa, B., Sammonds, P., Luckman, A., King, E., & Glasser, N. F. (2010). Present stability of the Larsen C Ice Shelf, Antarctic Peninsula. *Journal of Glaciology*, 56(198), 593–600. <https://doi.org/10.3189/002214310793146223>

Jansen, D., Luckman, A., Kullessa, B., Holland, P. R., & King, E. C. (2013). Marine ice formation in a suture zone on the Larsen C Ice Shelf and its influence on ice shelf dynamics. *Journal of Geophysical Research: Earth Surface*, 118(3), 1628–1640. <https://doi.org/10.1002/jgrf.20120>

Jansen, D., Luckman, A. J., Cook, A., Bevan, S., Kullessa, B., Hubbard, B., & Holland, P. R. (2015). Brief Communication: Newly developing rift in Larsen C Ice Shelf presents significant risk to stability. *The Cryosphere*, 9, 1223–1227. <https://doi.org/10.5194/tc-9-1223-2015>

Jenkins, A., & Bombosch, A. (1995). Modeling the effects of frazil ice crystals on the dynamics and thermodynamics of ice shelf water plumes. *Journal of Geophysical Research*, 100(C4), 6967–6981. <https://doi.org/10.1029/94jc03227>

Jenkins, A., Nicholls, K. W., & Corr, H. F. J. (2010). Observation and parameterization of ablation at the base of ronne ice shelf, Antarctica. *Journal of Physical Oceanography*, 40(10), 2298–2312. <https://doi.org/10.1175/2010jpo4317.1>

Jullion, L., Naveira Garabato, A. C., Meredith, M. P., Holland, P. R., Courtis, P., & King, B. A. (2013). Decadal freshening of the Antarctic bottom water exported from the Weddell Sea. *Journal of Climate*, 26(20), 8111–8125. <https://doi.org/10.1175/jcli-d-12-00765.1>

Kullessa, B., Booth, A. D., O’Leary, M., McGrath, D., King, E. C., Luckman, A. J., & Hubbard, B. (2019). Seawater softening of suture zones inhibits fracture propagation in Antarctic ice shelves. *Nature Communications*, 10(5491). <https://doi.org/10.1038/s41467-019-13539-x>

Kullessa, B., Jansen, D., Luckman, A. J., King, E. C., & Sammonds, P. R. (2014). Marine ice regulates the future stability of a large Antarctic ice shelf. *Nature Communications*, 5(1), 1–7. <https://doi.org/10.1038/ncomms4707>

Lambrecht, A., Sandhäger, H., Vaughan, D. G., & Mayer, C. (2007). New ice thickness maps of Filchner-Ronne Ice Shelf, Antarctica, with specific focus on grounding lines and marine ice. *Antarctic Science*, 19(4), 521–532. <https://doi.org/10.1017/s0954102007000661>

- Larour, E., Rignot, E., Poinelli, M., & Scheuchl, B. (2021). Physical processes controlling the rifting of Larsen C Ice Shelf, Antarctica, prior to the calving of iceberg A68. *Proceedings of the National Academy of Sciences*, 118(40). <https://doi.org/10.1073/pnas.2105080118>
- Losch, M. (2008). Modeling ice shelf cavities in a z coordinate ocean general circulation model. *Journal of Geophysical Research*, 113(C8). <https://doi.org/10.1029/2007jc004368>
- Marshall, J., Adcroft, A., Hill, C., Perelman, L., & Heisey, C. (1997). A finite-volume, incompressible Navier Stokes model for studies of the ocean on parallel computers. *Journal of Geophysical Research*, 102(C3), 5753–5766. <https://doi.org/10.1029/96jc02775>
- McGrath, D., Steffen, K., Holland, P. R., Scambos, T., Rajaram, H., Abdalati, W., & Rignot, E. (2014). The structure and effect of suture zones in the Larsen C Ice Shelf, Antarctica. *Journal of Geophysical Research: Earth Surface*, 119(3), 588–602. <https://doi.org/10.1002/2013jf002935>
- Mouginot, J., Scheuchl, B., & Rignot, E. (2012). Mapping of ice motion in Antarctica using synthetic-aperture radar data. *Remote Sensing*, 4(9), 2753–2767. <https://doi.org/10.3390/rs4092753>
- Mueller, R. D., Padman, L., Dinniman, M. S., Erofeeva, S. Y., Fricker, H. A., & King, M. A. (2012). Impact of tide-topography interactions on basal melting of Larsen C Ice Shelf, Antarctica. *Journal of Geophysical Research*, 117(C5). <https://doi.org/10.1029/2011jc007263>
- Mulvaney, R., Abram, N. J., Hindmarsh, R. C., Arrowsmith, C., Fleet, L., Triest, J., & Foord, S. (2012). Recent Antarctic Peninsula warming relative to Holocene climate and ice-shelf history. *Nature*, 489(7414), 141–144. <https://doi.org/10.1038/nature11391>
- Neal, C. (1979). The dynamics of the Ross Ice Shelf revealed by radio echo-sounding. *Journal of Glaciology*, 24(90), 295–307. <https://doi.org/10.3189/s0022143000014817>
- Nicholls, K. W., Makinson, K., & Venables, E. J. (2012). ocean circulation beneath Larsen C Ice Shelf, Antarctica from *in situ* observations. *Geophysical Research Letters*, 39(19). <https://doi.org/10.1029/2012gl053187>
- Nicholls, K. W., Pudsey, C. J., & Morris, P. (2004). Summertime water masses off the northern Larsen C Ice Shelf, Antarctica. *Geophysical Research Letters*, 31(9). <https://doi.org/10.1029/2004gl019924>
- Oerter, H., Kipfstuhl, J., Determann, J., Miller, H., Wagenbach, D., Minikin, A., & Graft, W. (1992). Evidence for basal marine ice in the filchner-ronne ice shelf. *Nature*, 358, 399–401. <https://doi.org/10.1038/358399a0>
- Rignot, E., Mouginot, J., & Scheuchl, B. (2011). Ice flow of the Antarctic ice sheet. *Science*, 333(6048), 1427–1430. <https://doi.org/10.1126/science.1208336>
- Robin, G. de Q. (1979). Formation, flow, and disintegration of ice shelves. *Journal of Glaciology*, 24(90), 259–271. <https://doi.org/10.1017/s0022143000014787>
- Schannwell, C., Cornford, S., Pollard, D., & Barrand, N. E. (2018). Dynamic response of Antarctic peninsula ice sheet to potential collapse of larsen C and george VI ice shelves. *The Cryosphere*, 12(7), 2307–2326. <https://doi.org/10.5194/tc-12-2307-2018>
- Shepherd, A., Wingham, D., Payne, T., & Skvarca, P. (2003). Larsen ice shelf has progressively thinned. *Science*, 302(5646), 856–859. <https://doi.org/10.1126/science.1089768>
- Skvarca, P., Rack, W., Rott, H., & Donangelo, T. I. Y. (1998). Evidence of recent climatic warming on the eastern Antarctic Peninsula. *Annals of Glaciology*, 27, 628–632. <https://doi.org/10.3189/s0260305500018164>
- Turner, J., Lu, H., White, I., King, J. C., Phillips, T., Hosking, J. S., & Deb, P. (2016). Absence of 21st century warming on Antarctic Peninsula consistent with natural variability. *Nature*, 535(7612), 411–415. <https://doi.org/10.1038/nature18645>
- Vaughan, D. G., Marshall, G. J., Connolley, W. M., Parkinson, C., Mulvaney, R., Hodgson, D. A., & Turner, J. (2003). Recent rapid regional climate warming on the Antarctic peninsula. *Climatic Change*, 60(3), 243–274. <https://doi.org/10.1023/a:1026021217991>

References From the Supporting Information

- Codiga, D. L. (2011). *Unified tidal analysis and prediction using the utide matlab functions*. Graduate School of Oceanography, University of Rhode Island Narragansett.
- King, M. A., Padman, L., Nicholls, K., Clarke, P. J., Gudmundsson, G. H., Kulesa, B., & Shepherd, A. (2011). Ocean tides in the Weddell Sea: New observations on the Filchner-Ronne and Larsen C Ice Shelves and model validation. *Journal of Geophysical Research*, 116(C6), 1–18. <https://doi.org/10.1029/2011JC006949>